Quantum waveguide theory for mesoscopic structures

Jian-Bai Xia
Chinese Center of Advanced Science and Technology (World Laboratory), P.O. Box 8730, Beijing 100080, China and Institute of Semiconductors, Chinese Academy of Sciences, P.O. Box 912, Beijing 100083, China
(Received 19 July 1991; revised manuscript received 23 September 1991)

A one-dimensional quantum waveguide theory for mesoscopic structures is proposed, and the boundary conditions of the wave functions at an intersection are given. The Aharonov-Bohm effect is quantitatively discussed with use of this theory, and the reflection, transmission amplitudes, etc., are given as functions of the magnetic flux, the arm lengths, and the wave vector. It is found that the oscillating current consists of a significant component of the second harmonic. This theory is also applied to investigate quantum-interference devices. The results on the Aharonov-Bohm effect and the quantum-interference devices are found to be in agreement with previous theoretical results.

I. INTRODUCTION

Since the Aharonov-Bohm effect was experimentally verified by Webb *et al.*,[1] there have been many advances in the physics of mesoscopic structures. The discussion of the Aharonov-Bohm effect was based on the theory of small normal one-dimensional rings,[2] and a generalized many-channel conductance theory[3] proposed by Büttiker *et al.*[4] Most of the initial work on electron transport in small systems has dealt with metallic samples, in which many transverse subbands were involved and the transport was diffusive. More recently, advances in semiconductor microtechnology have made it possible to fabricate extremely high-mobility quantum wires with narrow widths, in which only a few of the lowest subbands are occupied and the transport is ballistic. The allowed modes in the channel are then the "waveguide" modes.

The splitting-gate structure experiments[5,6] verified the waveguide characteristics of electron transport through a wide-narrow-wide structure. Kirczenov[7] made a detailed quantum-mechanical calculation for this structure, and explained the fine structure of the conductance plateaus observed in the experiments. Datta and Bandyopadhyay[8] presented a simple theory for the Aharonov-Bohm effect in semiconductor microstructures, assuming ballistic transport. It was shown that in well-designed symmetric structures it may be possible to attain large conductance modulation in a magnetic field even if the transverse dimension of the structure is large, the aspect is poor, and $k_B T$ exceeds the correlation energy. Many of the device concepts based on the quantum-interference effect have been proposed in the past few years.[9,10] Sols *et al.*[11] presented a theoretical study of semiconductor T structures that may exhibit transistor action. The calculation showed that relatively small changes in the stub length can induce strong variations in the electron transmission across the structure. The performance of the device can be improved by inserting additional stubs of slightly different lengths. Obviously, for a full understanding of the physics of mesoscopic structures of waveguide type, the solution of the one-electron Schrödinger equation

$$\left[-\frac{\hbar^2}{2m^*}\nabla^2+V(\mathbf{r})\right]\psi(\mathbf{r})=E\psi(\mathbf{r}) \tag{1}$$

is necessary.

In this paper we present a one-dimensional quantum waveguide theory for the mesoscopic structures of waveguide type, and apply it to the Aharonov-Bohm effect and other quantum-interference devices.

II. QUANTUM WAVEGUIDE THEORY FOR MESOSCOPIC STRUCTURES

The starting point is the Schrödinger equation (1). We assume that the width of the structure is narrow enough compared to the length of the structure so that the energy spacing between the quantum energy levels produced by the transverse confinement is much larger than the energy range of the longitudinal transport. Therefore, Eq. (1) reduces to a one-dimensional equation with the coordinate axis along the longitudinal direction of the structure.

One main problem is the boundary conditions at an intersection crossed by more than two circuits. Let ψ_i be the wave function in the ith circuit; then, at the intersection, the continuity of the wave functions demands that

$$\psi_1=\psi_2=\psi_3=\cdots=\psi_n \ . \tag{2}$$

From the conservation of the current density we obtain

$$\sum_i \frac{\alpha\psi_i}{\alpha x_i}=0 \ , \tag{3}$$

where all the coordinates x point to or point back to the intersection.

The wave function in each circuit is the linear combination of two plane waves with opposite wave vectors,

$$\psi_i(x)=c_{1i}e^{ikx}+c_{zi}e^{-ikx} \ . \tag{4}$$

There are $2n$ unknown coefficients for the n circuits crossing the intersection, among which the n coefficients can be determined by the n equations (2) and (3); the oth-

er half of the coefficients will be determined by the boundary conditions at the other intersections or the conditions at the input or output terminals. Hence the set of equations (2) and (3) at all cross points is complete for determining the wave function of the whole structure.

III. RING WITH TWO LEADS

To illustrate the application of the above theory, we consider the structure of a ring with two leads as shown in Fig. 1(a) in the absence of magnetic field. The two arms of the ring have different lengths L_1 and L_2. We introduce the local coordinate system for each circuit such that the direction is along the electron-current direction and the origin is taken at the intersection of the upper reaches. For the input circuit, the coordinate origin is taken at the intersection of the lower reaches. The choice of the coordinate origin is noncritical; it only affects a phase factor on the wave function.

In the local coordinate system, the wave functions in the circuits 1–4 shown in Fig. 1(a) can be written as

$$\begin{aligned}
\psi_1 &= e^{ikx} + a e^{-ikx} , \\
\psi_2 &= c_1 e^{ikx} + c_2 e^{-ikx} , \\
\psi_3 &= d_1 e^{ikx} + d_z e^{-ikx} , \\
\psi_4 &= g e^{ikx} ,
\end{aligned} \tag{5}$$

where we assumed that an electron with wave vector k enters in circuits 1 and departs from circuits 4, thus the coefficients a and g are the reflection and transmission amplitudes, respectively.

The boundary condition equations (2) and (3) for the wave functions (5) can be written at the A and B points,

$$\begin{aligned}
&1 + a = c_1 + c_2 , \\
&1 + a = d_1 + d_2 , \\
&1 - a = c_1 - c_2 + d_1 - d_2 , \\
&c_1 e^{ikL_1} + c_2 e^{-ikL_1} = g , \\
&d_1 e^{ikL_2} + d_2 e^{-ikL_2} = g , \\
&c_1 e^{ikL_1} - c_2 e^{-ikL_1} + d_1 e^{ikL_2} - d_2 e^{-ikL_2} = g .
\end{aligned} \tag{6}$$

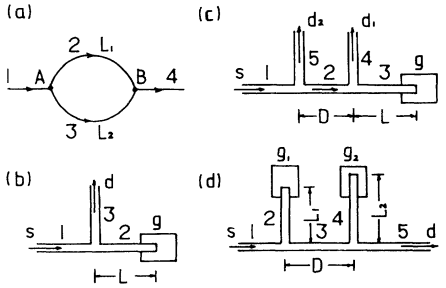

FIG. 1. Various configurations of the mesoscopic structures: (a) ring with two arms; (b) quantum-interference transistor; (c) quantum-interference device with two drains; (d) quantum-interference device with two gates. s, g, and d represent the source, gate, and drain, respectively.

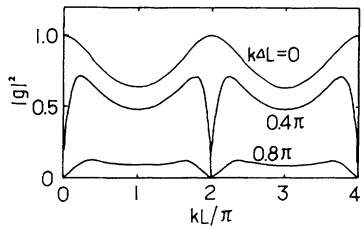

FIG. 2. $|g|^2$ as functions of kL for different $k\,\Delta L$ in the structure shown in Fig. 1(a) without magnetic field.

From Eq. (6) we obtain

$$\begin{aligned}
a &= \frac{1}{\Delta_L}(-8 + 3e^{ikL} + 3e^{-ikL} + e^{ik\,\Delta L} + e^{-ik\,\Delta L}) , \\
c_1 &= \frac{2}{\Delta_L}(2 - 3e^{-ikL} + e^{ik\,\Delta L}) , \\
c_2 &= \frac{2}{\Delta_L}(-2 + e^{ikL} + e^{-ik\,\Delta L}) , \\
d_1 &= \frac{2}{\Delta_L}(2 - 3e^{-ikL} + e^{-ik\,\Delta L}) , \\
d_2 &= \frac{2}{\Delta_L}(-2 + e^{ikL} + e^{ik\,\Delta L}) , \\
g &= \frac{16i}{\Delta_L}\sin\left[k\frac{L}{2}\right]\cos\left[k\frac{\Delta L}{2}\right] ,
\end{aligned} \tag{7}$$

where

$$L = L_1 + L_2 , \quad \Delta L = L_2 - L_1 , \tag{8}$$

$$\Delta_L = 8 - e^{ikL} - 9e^{-ikL} + e^{ik\,\Delta L} + e^{-ik\,\Delta L} .$$

From Eq. (7) we obtain the current proportional to

$$\begin{aligned}
|g|^2 &= \frac{64}{\Delta_L^2}[1 - \cos(kL)][1 + \cos(k\,\Delta L)], \\
\Delta_L^2 &= 4\{[4 - 5\cos(kL) + \cos(k\,\Delta L)]^2 + [4\sin(kL)^2]\} .
\end{aligned} \tag{9}$$

It is expected that the conductance will change periodically as L is changed for a fixed ΔL, or as ΔL is changed for a fixed L. The former result cannot be obtained if we simply consider the overlap of two plane waves. The $|g|^2$ as a function of kL for fixed $k\,\Delta L$ and as a function of $k\,\Delta L$ for fixed kL are shown in Figs. 2 and 3, respective-

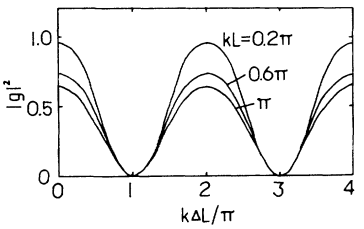

FIG. 3. $|g|^2$ as functions of $k\,\Delta L$ for different kL in the structure shown in Fig. 1(a) without magnetic field.

ly. From the figures we see that the oscillations of $|g|^2$ with $k\,\Delta L$ are better than that with kL.

IV. AHARONOV-BOHM RING

The structure of the Aharonov-Bohm ring is the same as that in Fig. 1(a). In the magnetic field, the Schrödinger equation (1) is replaced by

$$\left[\frac{1}{2m^*}\left[\mathbf{P}+\frac{e}{c}\mathbf{A}\right]^2+V(\mathbf{r})\right]\psi(\mathbf{r})=E\psi(\mathbf{r}) , \tag{10}$$

where $\mathbf{A}$ is the vector potential of the magnetic field $\mathbf{B}$,

$$\mathbf{A}=\nabla\times\mathbf{B} . \tag{11}$$

As the magnetic field $\mathbf{B}$ is perpendicular to the ring plane, according to the Gauss theorem the vector potential $\mathbf{A}$ is along the ring direction, and its magnitude

$$A=\frac{\Phi}{L} , \tag{12}$$

where $\Phi=B\cdot S$ is the magnetic flux through the ring section area S, and L is the ring round length.

Inserting (12) into Eq. (10), we obtain the one-dimensional Schrödinger equation,

$$\left[\frac{1}{2m^*}\left[\frac{\hbar}{i}\frac{d}{dx}-\frac{e}{c}\frac{\Phi}{L}\right]^2+V(x)\right]\psi(x)=E\psi(x) . \tag{13}$$

The wave function $\psi(x)$ is still a plane wave with wave vector k_1, its eigenenergy

$$E=\frac{\hbar^2}{2m^*}\left[k_1-\frac{e\Phi}{\hbar cL}\right]^2 , \tag{14}$$

which should be equal to the energy of the injected electron, $\hbar^2k^2/2m^*$. Thus we have

$$k_1=k+\frac{e\Phi}{\hbar cL} . \tag{15}$$

For the electron moving in the opposite direction to the $\mathbf{A}$, we obtain the wave vector of the electron

$$k_2=k-\frac{e\Phi}{\hbar cL} . \tag{16}$$

The wave functions in the circuits 1–4 shown in Fig. 1(a) are written as

$$\begin{aligned}
&\psi_1=e^{ikx}+ae^{-ikx} ,\\
&\psi_2=c_1e^{ik_1x}+c_2e^{-ik_2x} ,\\
&\psi_3=d_1e^{ik_2x}+d_2e^{-ik_1x} ,\\
&\psi_4=ge^{ikx} ,
\end{aligned} \tag{17}$$

where the k_1 and k_2 are given in Eqs. (15) and (16), respectively. Similarly, we can write down the boundary-condition equations at the A and B points, and obtain

$$\begin{aligned}
a=&\frac{1}{\Delta_k}\left[e^{-ik_1\Delta L}+e^{ik_2\Delta L}-(k_1+k_2)^2(e^{-i\Delta kL_1}+e^{i\Delta kL_2})\right.\\
&-(1+k_1+k_2)(1-k_1-k_2)\\
&\left.\times(e^{-ik_2L_1-ik_1L_2}+e^{ik_1L_1+ik_2L_2})\right] .\\
c_1=&\frac{2}{\Delta_k}\left[e^{ik_2\Delta L}+(k_1+k_2)e^{i\Delta kL_2}\right.\\
&\left.-(1+k_1+k_2)e^{-ik_1L_2-ik_2L_1}\right] ,\\
c_2=&\frac{2}{\Delta_k}\left[e^{-ik_1\Delta L}-(k_1+k_2)e^{i\Delta kL_2}\right.\\
&\left.-(1-k_1-k_2)e^{ik_1L_1+ik_2L_2}\right] ,\\
d_1=&\frac{2}{\Delta_k}\left[e^{-ik_1\Delta L}+(k_1+k_2)e^{-i\Delta kL_1}\right.\\
&\left.-(1+k_1+k_2)e^{-ik_1L_2-ik_2L_1}\right] ,\\
d_2=&\frac{2}{\Delta_k}\left[e^{ik_2\Delta L}-(k_1+k_2)e^{-i\Delta kL_1}\right.\\
&\left.-(1-k_1-k_2)e^{ik_1L_1+ik_2L_2}\right] ,\\
g=&\frac{2(k_1+k_2)}{\Delta_k}\left[e^{ik_1L_1-ik_2L_1+ik_2L_2}-e^{ik_1L_1-ik_1L_2-ik_2L_1}\right.\\
&+e^{ik_1L_1-ik_1L_2+ik_2L_2}\\
&\left.-e^{ik_1L_2-ik_2L_1+ik_2L_2}\right] ,
\end{aligned} \tag{18}$$

where

$$\begin{aligned}
&K_1=\frac{k_1}{k} , \quad K_2=\frac{k_2}{k} , \quad \Delta k=k_2-k_1 ,\\
&\Delta_k=e^{ik_1\Delta L}+e^{ik_2\Delta L}+(k_1+k_2)^2(e^{-i\Delta kL_1}+e^{i\Delta kL_2})\\
&\quad-(1+k_1+k_2)^2e^{-ik_1L_2-ik_2L_1}\\
&\quad-(1-k_1-k_2)^2e^{ik_1L_1+ik_2L_2} .
\end{aligned} \tag{19}$$

Under the approximation

$$L_1=L_2=\frac{L}{2} , \quad K_1\approx K_2\approx 1 , \tag{20}$$

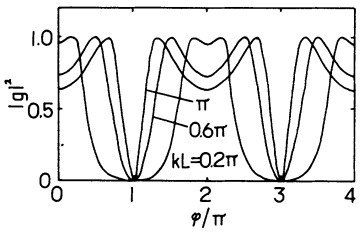

FIG. 4. $|g|^2$ as functions of φ for different kL in the Aharonov-Bohm ring.

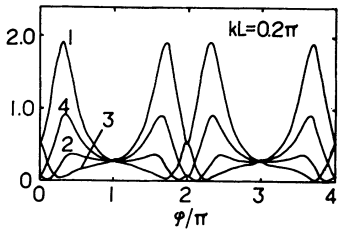

FIG. 5. Squared amplitudes of wave functions in two arms of the Aharonov-Bohm ring for $kL=0.2\pi$. Curves 1, 2, 3, and 4 represent $|c_1|^2$, $|c_2|^2$, $|d_1|^2$, and $|d_2|^2$, respectively.

Eqs. (18) and (19) can be simplified, and give

$$|g|^2=\frac{64}{\Delta_k^2}(1-\cos kL)(1+\cos\psi)\ ,$$

$$\Delta_k^2=4[(1+4\cos\psi-5\cos kL)^2+(4\sin kL)^2]\ , \tag{21}$$

$$\psi=\Delta k\,\frac{L}{2}=-\frac{e\Phi}{\hbar c}\ .$$

From Eq. (21) we see that the $|g|^2$ changes periodically as φ is changed with the period

$$\Phi=\frac{hc}{e}\ . \tag{22}$$

This is the basic result of the Aharonov-Bohm effect, which is in agreement with the results of Datta and Bandyopadhyay.[8] The $|g|^2$ as functions of φ for several kL values are shown in Fig. 4. From the figure we see that the wave shape is good for kL close to zero (except for a factor of $2\pi n$; in the following and in figures we will use this abbreviation), but is bad for kL close to π, indicating that there are components of higher harmonics. Comparing Fig. 4 with Fig. 3, we found that the oscillations of $|g|^2$ with φ and $k\,\Delta L$ are very different. The difference comes from the Δ_k^2 in Eq. (21) and Δ_L^2 in Eq. (9): in Eq. (9) the factor of the $\cos(k\Delta L)$ term is 1, while in Eq. (21) the factor of the $\cos\varphi$ term is 4; the slight change of the $\cos\varphi$ will influence Δ_k, and hence the $|g|^2$, dramatically.

By using the Fourier transform we can calculate the nth harmonic component of the $|g|^2$,

$$I_n=\frac{1}{\pi}\int_0^{2\pi}|g|^2\cos(n\varphi)d\varphi\ . \tag{23}$$

From Eqs. (9) and (21), I_n can be written as

$$I_n=\mathrm{Re}\left[\frac{P}{\pi}\int_0^{2\pi}\frac{\cos(n\varphi)}{\cos\varphi+Q}d\varphi\right]\ , \tag{24}$$

where P and Q are complex constants. Let $z=e^{i\varphi}$; the integral in Eq. (24) can be calculated by the complex variable integral of z along a unit circle in the complex plane. The results are

$$\frac{1}{\pi}\int_0^{2\pi}\frac{\cos\varphi}{\cos\varphi+Q}d\varphi=\frac{4\alpha}{\alpha-\beta}\ , \tag{25}$$

$$\frac{1}{\pi}\int_0^{2\pi}\frac{\cos2\varphi}{\cos\varphi+Q}d\varphi=2\left[-2Q+\frac{\alpha^2+\beta^2}{\alpha-\beta}\right]\ , \tag{26}$$

where α and β are roots of the algebraic equation

$$z^2+2Qz+1=0\ ,$$

and $|\alpha|<1$, $|\beta|>1$.

The calculated I_1 and I_2 for the $k\,\Delta L$ oscillation [Eq. (9)] and the φ oscillation [Eq. (21)] are shown in Table I for different kL values in the range $0-\pi$. From the table we see that for the $k\,\Delta L$ oscillation the I_2 is only one-tenth of the I_1, and the magnitudes of I_1 and I_2 are basically unvaried in the whole range of kL. For the φ oscillation the I_1 decreases, and the ratio of I_2 to I_1 increases as kL increases from zero to π. Physically, the large I_2 component comes from the fact that the waves move in opposite directions with different wave vectors k_1 and k_2 [Eqs. (15) and (16)].

The squared amplitudes of waves in the upper and lower arms of the ring $|c_1|^2$, $|c_2|^2$, $|d_1|^2$, and $|d_2|^2$ as functions of φ for $kL=0.2\pi$ and π are shown in Figs. 5 and 6, respectively. From the figures we see that in the case of the good oscillation $kL=0.2\pi$, the $|c_1|^2$ and $|d_2|^2$ are large, and the $|c_1|^2$ exceeds 1, indicating that the electron makes a cyclotron motion in the ring. In the case of $kL=\pi$, the $|c_1|^2$ equals $|d_1|^2$, and $|c_2|^2$ equals $|d_2|^2$; the electrons in the two arms move parallel to the output lead.

TABLE I. Harmonic components I_1 and I_2 of $|g|^2$ as functions of kL for the $k\,\Delta L$ and φ oscillations.

	kL	0.05	0.10	0.15	0.20	0.30	0.40	0.50
$k\,\Delta L$	I_1	0.5329	0.4945	0.4523	0.4167	0.3615	0.3279	0.3168
	I_2	0.0584	−0.0390	−0.0603	−0.0604	−0.0489	−0.0403	−0.0375
φ	I_1	0.4631	0.5520	0.5566	0.5073	0.3229	0.1393	0.0645
	I_2	0.2524	0.1343	−0.0198	−0.1630	−0.3195	−0.2993	−0.2581

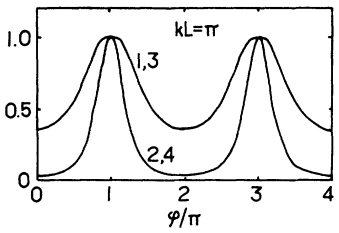

FIG. 6. Same as Fig. 5 but for $kL=\pi$.

V. QUANTUM-INTERFERENCE DEVICES

The quantum-interference transistor[9,10] as shown in Fig. 1(b) differs from the ordinary field-effect transistor (FET) in that the gate lies outside the classical path of the electrons. Conductive oscillations as a function of the gate potential have been observed in such a structure. The wave functions in the circuits 1–3 [Fig. 1(b)] can be written as

$$\begin{aligned}\psi_1&=e^{ikx}+ae^{-ikx}\ ,\\ \psi_2&=c\sin[k(x-L)]\ ,\\ \psi_3&=ge^{ikx}\ .\end{aligned}\tag{27}$$

Applying the boundary condition Eqs. (2) and (3), we obtain

$$\begin{aligned}&1+a=-c\sin(kL)\ ,\\ &1+a=g\ ,\\ &1-a+ic\cos(kL)=g\ .\end{aligned}\tag{28}$$

From Eq. (28) it is easy to obtain

$$\begin{aligned}a&=-\frac{i\cos(kL)}{2\sin(kL)+i\cos(kL)}\ ,\\ g&=\frac{2\sin(kL)}{2\sin(kL)+i\cos(kL)}\ .\end{aligned}\tag{29}$$

The $|g|^2$ as a function of kL is shown in Fig. 7 (dashed line). It can be seen that the wave shape is in good agreement with the experimental single-mode results.[9] It should be noted that this structure [Fig. 1(b)] is not the special case of the ring with two arms [Fig. 1(a)], taking $L_1=0$ and $L_2=2L$. In circuit 2 connecting the gate, the electronic wave function is a standing wave with the zero point at the gate. Therefore, the wave shapes for the two oscillations (Figs. 3 and 7) are completely different.

As a development of the interference device, we consider the structure with two drains controlled by one gate as shown in Fig. 1(c), and the two drains apart from a distance D. The wave functions in the circuits 1–5 can be written as

$$\begin{aligned}\psi_1&=e^{ikx}+ae^{-ikx}\ ,\\ \psi_2&=c_1e^{ikx}+c_2e^{-ikx}\ ,\\ \psi_3&=d\sin[k(x-L)]\ ,\\ \psi_4&=g_1e^{ikx}\ ,\\ \psi_5&=g_2e^{ikx}\ .\end{aligned}\tag{30}$$

Similarly we obtain,

$$\begin{aligned}a&=-\frac{1}{\Delta_D}\{[2\sin(kL)+i\cos(kL)]e^{-ikD}\\ &\quad+i\cos(kL)e^{ikD}\}\ ,\\ d&=-\frac{4}{\Delta_D}\ ,\\ g_1&=\frac{4}{\Delta_D}\sin(kL)\ ,\\ g_2&=\frac{2}{\Delta_D}\{[2\sin(kL)+i\cos(kL)]e^{-ikD}\\ &\quad-i\cos(kL)e^{ikD}\}\ ,\\ \Delta_D&=3[2\sin(kL)+i\cos(kL)]e^{-ikD}-i\cos(kL)e^{ikD}\ .\end{aligned}\tag{31}$$

The $|g_1|^2$ and $|g_2|^2$ as functions of kL for three kD values are shown in Figs. 7 and 8, respectively. From Fig. 7 we see that in the drain near to the gate, the current oscillations are nearly the same, independent of kD, and their magnitudes are about half of that in the single-drain structure (dashed line). In the drain far away from the gate, the current oscillations critically depend on the kD, and they have opposite phases for the cases of $kD=0$ and 0.5π.

Finally, we consider a double-gate structure as shown in Fig. 1(d); the two stubs are apart by a distance D, and the lengths L_1 and L_2 of the stubs are controlled by the gate voltages. The wave functions in the circuits 1–5 are written as

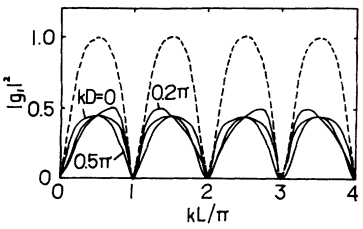

FIG. 7. $|g|^2$ as functions of kL for different kD in the first drain of the structure shown in Fig. 1(c). The dashed line is the $|g|^2$ in the structure shown in Fig. 1(b).

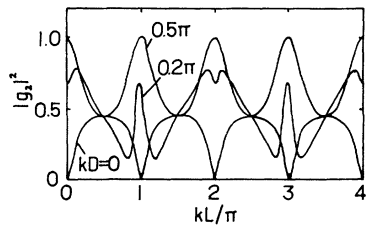

FIG. 8. $|g|^2$ as functions of kL for different kD in the second drain of the structure shown in Fig. 1(c).

$$\psi_1 = e^{ikx} + ae^{-ikx} ,$$
$$\psi_2 = b \sin k(x - L_1) ,$$
$$\psi_3 = c_1 e^{ikx} + c_2 e^{-ikx} , \tag{32}$$
$$\psi_4 = d \sin[k(x - L_2)] ,$$
$$\psi_5 = g e^{ikx} .$$

We obtain

$$a = -\frac{2i}{\Delta_{D,L}} [\sin(kL_1)\cos(kL_z) e^{ikD} + \cos(kL_1)\sin(kL_2) e^{-ikD} + \cos(k, L_1)\cos(kL_2)\sin(kD)] ,$$
$$g = \frac{4}{\Delta_{D,L}} \sin(kL_1)\sin(kL_2) , \tag{33}$$
$$\Delta_{D,L} = [4\sin(kL_1)\sin(kL_2) + 2i\cos(kL_1)\sin(kL_2) + 2i\sin(kL_1)\cos(kL_2)] e^{-ikD} + 2i\cos(kL_1)\cos(kL_2)\sin(k_D) .$$

For comparison with the theoretical results of the ideal two-dimensional electron waveguide model,[11] we calculated the transmission probability $|g|^2$ for the single- and double-gate structures with the same parameters as in Ref. 11. Of course, the width effect is neglected in our model. We take the electron effective mass $m^* = 0.05 m_0$, electron energy $E \approx 0.08$ eV, and the separation between two stubs $D = 95$ Å. In Fig. 9 the $|g|^2$ for the structures of a single stub, two identical stubs, and two stubs with length difference $\Delta L = 10$ Å are given, respectively. From the figure we see that they are qualitatively in agreement with the two-dimensional theoretical model results for the structure with equal width.[11] In the case of single stub, the transmission valley is narrow, while in the case of two identical stubs the valley becomes broader. In the case of two stubs of different lengths, there appears an additional peak at the transmission valley, and the valley is broadened further. It is found that the peak height is sensitive to the kD, and the $|g|^2$ as functions of kL^* for $kD = 3.0$, π, and 3.3 are shown in Fig. 9(d), corresponding to wave lengths $\lambda = 200$, 190, and 180 Å, respectively. From the figure we see that if $kD = \pi$, there is a strong resonant peak at the transmission valley; if kD deviates from π, the resonant peak decreases greatly. There are some differences between our pure one-dimensional results and the two-dimensional results. Except for the wave form of $|g|^2$, in the one-dimensional case the oscillation period is unchanged, while in the two-dimensional case the period changes from one period to another due to the width effect. In the above calculation we have assumed that the electron wave has a wave node at the gate, hence in the stub the wave function has the form of $\sin[k(x - L)]$, where L is the length of the stub. As a result, the transmission probability $|g|^2$ is zero as kL approaches zero. If we assume that the electron wave has a wave peak at the gate, then the wave function in the stub has the form of $\cos[k(x - L)]$. All the above results change with $\sin kL$ replaced by $-\cos kL$, and $\cos kL$ replaced by $\sin kL$. This means that the kL shifts by $\pi/2$ relative to the original one, and the $|g|^2$ does not equal zero as kL approaches zero. This case is shown in Fig. 9.

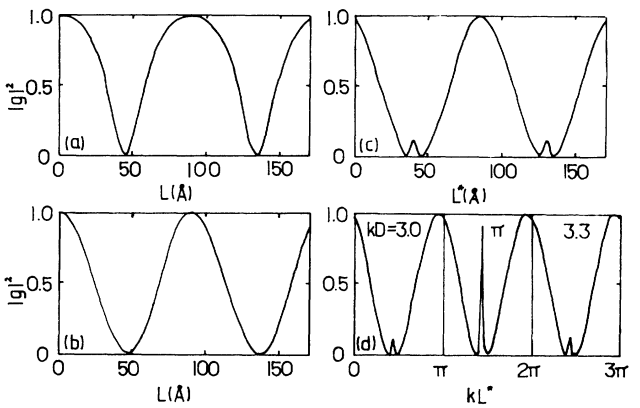

FIG. 9. $|g|^2$ as functions of L for the structures of (a) a single stub, (b) two identical stubs, and (c) two stubs with length difference $\Delta L = 10$ Å. In case (c) L^* refers to the shorter one, $k = 0.0347$ Å, $D = 95$ Å. (d) $|g|^2$ as functions of kL^* for $kD = 3.0$, π, and 3.3.

VI. SUMMARY

In summary, we have presented a one-dimensional quantum waveguide theory for the waveguide-type mesoscopic structures. We have given the boundary conditions of the wave functions at the intersections, which guarantee the continuity of wave functions and the conservation of current densities. With this theory we have discussed quantitatively the Aharonov-Bohm effect, giving the reflection, transmission, and other wave-function amplitudes in the ring as functions of the magnetic flux, the arm lengths, and the electronic wave vector. It is found that the oscillating current consists of a significant component of the second harmonics, especially as kL approaches π. The quantum waveguide theory was also applied to investigate the quantum-interference devices. The conductance oscillations as functions of kL and kD in the case of single-gate, double-drain, and double-gate structures are discussed.

The one-dimensional quantum waveguide theory, though neglecting the width effect, gives the main results, which are in agreement with the experiments and the results of more precise theory. It may be useful in analyzing complex systems with many intersections and branches.

ACKNOWLEDGMENT

This work was supported by the Chinese National Science Foundation.

[1]R. A. Webb, S. Washburn, C. P. Umbach, and R. B. Laibowitz, Phys. Rev. Lett. **54**, 2696 (1985).
[2]M. Buttiker, Y. Imry, and R. Landauer, Phys. Lett. **96A**, 365 (1983).
[3]Y. Gafen, Y. Imry, and M. Ya. Azbel, Phys. Rev. Lett. **52**, 129 (1984).
[4]M. Büttiker, Y. Imry, R. Landauer, and S. Pinkas, Phys. Rev. B **31**, 6207 (1985).
[5]B. J. van Wees, H. van Houten, C. W. J. Beenakker, J. G. Williamson, L. P. Konwenhoven, D. Van der Marel, and C. F. Foxon, Phys. Rev. Lett. **60**, 848 (1988).
[6]D. A. Wharam, T. J. Thornton, R. Newbury, M. Pepper, H. Ahmed, J. E. F. Frost, D. G. Hasko, D. C. Peacock, D. A. Ritchie, and G. A. C. Jones, J. Phys. C **21**, L **209** (1988).
[7]G. Kirczenov, Phys. Rev. B **39**, 10452 (1989).
[8]S. Datta and S. Bandyopadhyay, Phys. Rev. Lett. **58**, 717 (1987).
[9]S. Datta, Superlatt. Microstruct. **6**, 83 (1989).
[10]F. Capasso and S. Datta, Phys. Today **LB** (2), 74 (1990).
[11]F. Sols, M. Macucci, U. Ravaioli, and K. Hess, J. Appl. Phys. **66**, 3892 (1989).